

Flatness measurement using a grazing incidence interferometer

N. Alcalá Ochoa*, G. Mendiola, and J.E.A. Landgrave
*Centro de Investigaciones en Óptica,
 Apartado Postal 1-948, León, Guanajuato, México,
 e-mail: alon@foton.cio.mx

Recibido el 12 de agosto de 2005; aceptado el 30 de noviembre de 2006

The purpose of this work is to report results of flatness measurements using a grazing incidence interferometer. We show that this interferometer provides enough accuracy to measure nominally flat polishing tools and rough surfaces. In order to calculate the deformation of the surface under test, an interferogram is analyzed with digital imaging techniques based on Fourier methods. We found experimentally that the entire surface topography can be recovered with errors lower than $\sim 0.6\mu\text{m}$, or $\sim \lambda_{eqv}/6$, where $\lambda_{eqv} = 3.6441\mu\text{m}$ is the equivalent wavelength of the interferometer.

Keywords: Optical testing; interferometry; fringe analysis; laser applications.

El propósito de este trabajo es el de reportar resultados de medición de planicidad usando un interferómetro de incidencia oblicua. Se muestra que este interferómetro proporciona la exactitud necesaria para medir la planicidad de herramientas de pulido y superficies rugosas. Con el propósito de evaluar las irregularidades de la superficie bajo prueba, el interferograma obtenido se analiza con técnicas de procesamiento digital de imágenes basadas en métodos de Fourier. Encontramos experimentalmente que la superficie completa se puede medir con errores menores a $\sim 0.6\mu\text{m}$, o $\sim \lambda_{eqv}/6$, donde $\lambda_{eqv} = 3.6441\mu\text{m}$ es la longitud de onda equivalente del interferómetro.

Descriptores: Pruebas ópticas; interferometría; análisis de franjas; aplicaciones de láseres.

PACS: 06.20.-f; 42.62.-b; 42.62.Cf

1. Introduction

The optical testing of polished flat surfaces is a common practice in an optical workshop, and various interferometric devices are readily available for this purpose. However, when the surface under test is not specular, these devices are no longer useful. To deal with this problem, we developed a grazing incidence interferometer (GII) for our optical workshop at Centro de Investigaciones en Óptica (CIO) (Fig. 1)[1,2]. The principle behind this interferometer is that an unpolished surface becomes more reflective when the wavelength of the illuminating beam is increased. This reflection phenomenon is also observed when the surface under test is illuminated with a beam that makes a large angle with the normal to the surface. In this latter case we may speak of an equivalent wavelength. Relative to this equivalent wavelength, the surface appears polished enough to yield interference fringes.



FIGURE 1. Grazing Incidence Interferometer (GII) at CIO.

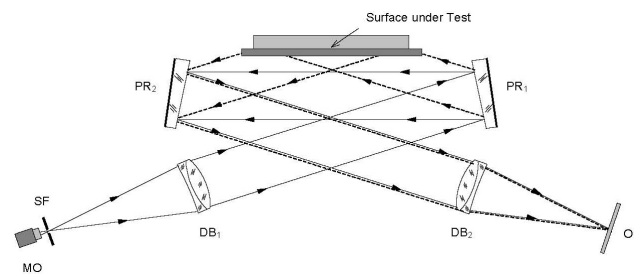


FIGURE 2. Schematic diagram of the GII at CIO.

Since the GII is an interferometer that produces fringes of equal thickness, a fringe pattern can be directly related to the departures of the surface under test from an ideal plane. Also, in common with other interferometers, during the alignment of the GII, carrier fringes can be introduced at will, making Fourier techniques a good candidate for the computation of the phase map associated with the fringe pattern. The main objective of this work was to prove that Fourier methods could in fact be used to reduce the data obtained with the GII, within tolerable error bounds.

In Secs. 2 and 3 of this work, we shall describe the GII at CIO, and the algorithm that we devised to reduce the data that we obtain with the interferometer. In Sec. 4 we shall present the results of testing a nominally flat specular surface with the GII, and also the results for a rough surface, prepared by grinding a glass surface with a $9\mu\text{m}$ abrasive.

2. Grazing incidence interferometer

Figure 2 shows a schematic drawing of the GII. The beam of a 10 mW He-Ne laser is expanded by a weak divergent lens (not shown) to fill the aperture of a low power microscope objective (MO). The objective focuses the beam at a spatial filter (SF) placed at the focal plane of a cemented doublet (DB₁), with a 62 mm clear diameter[3]. The doublet collimates the beam, which falls upon a prismatic beam splitter (PR₁). This has an apex angle of 7°, and was back coated with a reflective film to yield an intensity ratio of approximately 1:4 between the reference beam and the object beam. This latter beam illuminates the surface under test, which is placed on top of a metal plate with a 320 mm long by 32.5 mm wide rectangular aperture. The beam that is reflected from this surface enters a second prism (PR₂), which recombines this beam with the reference beam from the first prism (PR₁). Both collimated beams are focused at the focal plane of a second cemented doublet (DB₂). If we place ground glass at this plane, and bring together the two image points produced by both beams by means of adjustment screws at the metal plate that supports the surface under test, interference fringes can be seen in maxwellian view, that is, by placing the eye at the common focus of both beams (O). To do this we remove the ground glass that we used to align the interferometer, and place instead a polarizer to reduce the intensity of both beams to safe levels for direct viewing.

At a second stage in the development of the GII, an optoelectronic system was added in order to move from qualitative visual inspections to quantitative maps of the surface departures from an ideal plane. The system essentially consisted of a digital camera with 640×480 pixels and a Meteor II-MC frame grabber from Matrox, installed inside a personal computer (PC). To image the surface under test through the doublet DB₂, the lens in the camera was replaced by a low power microscope objective, attached to the camera C mount by means of a mechanical coupler, especially designed for this purpose. What we required was to image within the camera CCD, and with the largest possible magnification, the entire slot in the metal plate that supports the surface under test.

The optoelectronic system that we added to the GII allowed us to obtain digitized images of the interferograms in 256 gray levels. Now, by appropriately processing these images, we had to extract the topography of the surface under test.

3. Data reduction

The intensity distribution of the interferograms that we obtain with the GII can be written as

$$I(x, y) = I_r(x, y) + I_o(x, y) + 2\sqrt{I_r(x, y)I_o(x, y)} \cos \phi(x, y), \quad (1)$$

where $I_r(x, y)$ and $I_o(x, y)$ are, the reference and object beam intensities at the point with coordinates (x, y) in the

camera CCD, respectively, and $\phi(x, y)$ is the relative phase of the object beam at a reference plane. This plane is, of course, a “virtual” wave-front of the reference beam, more specifically, the wave-front that the reference beam would have at the surface under test, if an actual wave-front of this beam were propagated backwards until this surface.

We shall discuss next the method that we used to find the surface departures from an ideal plane, starting from the intensity distribution given by Eq. (1). There are several methods available for this purpose, known collectively as spatial methods[4-6]. We tried all of them with interferograms obtained from different kinds of polishing tools, and we found that the most versatile was the method based on Fourier-transform techniques[5], which was originally devised for interferograms of small domains and high fringe density.

Since the relative phase $\phi(x, y)$ depends on the orientation of the object wave-front with respect to a reference plane, and this plane can be chosen by a suitable manipulation of the interferometer, we can write

$$\phi(x, y) = \psi(x, y) + 2\pi(w_0x + w_1y), \quad (2)$$

where $\psi(x, y)$ is the relative phase of the object beam with the minimum variance,⁷ and w_0 and w_1 are tilt coefficients in the x and y directions, respectively. In our case, the values of w_0 and w_1 can be varied at will by adjusting the orientation of the metal plate that supports the surface under test, so that by this means we can introduce tilt fringes of any frequency and orientation into the interferogram. If the coefficients w_0 and w_1 are sufficiently large that

$$|\nabla\psi(x, y)| < 2\pi\sqrt{w_0^2 + w_1^2} \quad (3)$$

for all points (x, y) of the interferogram, there will not be an ambiguity in the order of interference corresponding to each fringe of the pattern. In this case, the fringe analysis is relatively simple. If, on the other hand, the condition in Eq. (3) is not fulfilled, more elaborate techniques are required to analyze the interferogram, such as phase-stepping and fringe regularization[8,9].

From Eqs. (1) and (2) we can write

$$I(x, y) = a(x, y) + c(x, y) \exp[i2\pi(w_0x + w_1y)] + c^*(x, y) \exp[-i2\pi(w_0x + w_1y)], \quad (4)$$

where

$$a(x, y) = I_r(x, y) + I_o(x, y), \quad (5)$$

and

$$c(x, y) = \sqrt{I_r(x, y)I_o(x, y)} \exp[i\psi(x, y)]. \quad (6)$$

The Fourier transform of $I(x, y)$ can then be written as

$$\hat{I}(u, v) = \hat{a}(u, v) + \hat{c}(u-w_0, v-w_1) + \hat{c}(u+w_0, v+w_1), \quad (7)$$

where u and v are the spatial frequencies in the x and y directions, and $\hat{f}(u, v) = F\{f(x, y)\}$, the symbol F denoting

Fourier transform. Since the spatial variations of $I_r(x, y)$, $I_o(x, y)$ and $\psi(x, y)$, and thus of the functions $a(x, y)$ and $c(x, y)$ [Eqs. (5) and (6)], can be assumed to be of a smaller

frequency than $\sqrt{w_0^2 + w_1^2}$, there will be practically no overlap among the three components of the spectrum $\hat{I}(u, v)$ in

Eq. (7). Consequently, by means of a window function $H(u-w_0, v-w_1)$ it is possible to filter out the function $\hat{c}(u-w_0, v-w_1)$ from the spectrum $\hat{I}(u, v)$. A subsequent translation to the origin yields $\hat{c}(u, v)$, and the inverse Fourier transform, $c(x, y)$. From Eq. (6) we can then obtain

$$\psi_+ = a \tan \left[\frac{\text{Im}\{c(x, y)\}}{\text{Re}\{c(x, y)\}} \right], \quad -\pi/2 < \psi_+ < +\pi/2, \quad (8)$$

so that the wrapped phase will be

$$\psi_w(x, y) = \begin{cases} \psi_+ & \text{if } \text{Re}\{c(x, y)\} > 0 \\ \psi_+ + \pi & \text{if } \text{Re}\{c(x, y)\} < 0 \text{ and } \text{Im}\{c(x, y)\} \geq 0 \\ \psi_+ - \pi & \text{if } \text{Re}\{c(x, y)\} < 0 \text{ and } \text{Im}\{c(x, y)\} < 0 \\ +\pi/2 & \text{if } \text{Re}\{c(x, y)\} = 0 \text{ and } \text{Im}\{c(x, y)\} > 0 \\ -\pi/2 & \text{if } \text{Re}\{c(x, y)\} = 0 \text{ and } \text{Im}\{c(x, y)\} < 0 \end{cases}, \quad (9)$$

with $-\pi < \psi_w \leq +\pi$.

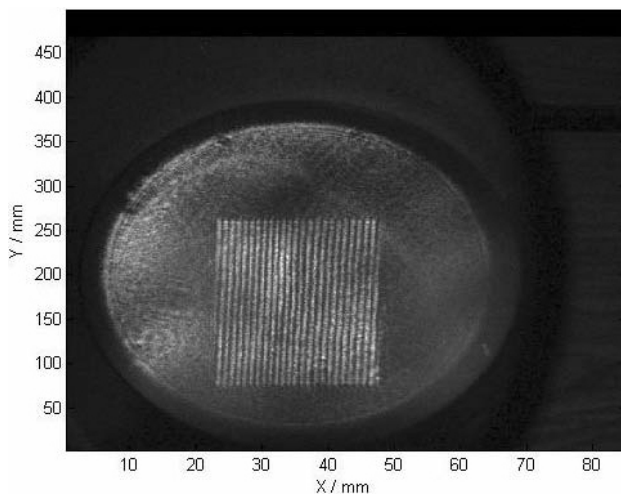


FIGURE 3. Interferogram obtained with the GII of a specular glass surface. This was from a 150×150 mm glass plate, placed on top of a metal plate with a 320 mm long by 32.5 mm wide rectangular aperture.

Let $D(x, y)$ be the function that accounts for the surface departures from an ideal plane, chosen as the plane that minimizes the variance of $D(x, y)$. If the gradient of $D(x, y)$ is assumed to be very small throughout the entire inspection area of the surface under test, the relative phase of the object wave-front can be approximated as

$$\psi(x, y) \approx 2\pi [2D(x, y) \cos \theta / \lambda], \quad (10)$$

where λ is the wavelength of the light source in the interferometer, and θ is the angle of incidence of the object beam on the surface under test[10]. Therefore

$$D(x, y) \approx \frac{\psi(x, y)}{4\pi} \lambda_{eqv}, \quad (11)$$

$$H(u - w_0, v - w_1) = \begin{cases} 0.54 + 0.46 \cos \left(\pi \sqrt{\frac{(u-w_0)^2}{a^2} + \frac{(v-w_1)^2}{b^2}} \right) & \text{if } \frac{(u-w_0)^2}{a^2} + \frac{(v-w_1)^2}{b^2} \leq 1 \\ 0 & \text{otherwise} \end{cases}, \quad (13)$$

where

$$\lambda_{eqv} = \lambda / \cos \theta \quad (12)$$

is the equivalent wavelength of the interferometer. The GII was designed to work with the object beam, making an angle $\theta = 80^\circ$ with the normal to the surface under test. With this value of θ and $\lambda = 0.6328 \mu\text{m}$, from Eq. (12) we obtain $\lambda_{eqv} = 3.6441 \mu\text{m}$.

4. Results

To verify the reliability of the method for data reduction outlined above, a window glass plate of 150×150 mm was tested in the GII, and the results compared with those obtained from a Wyko interferometer - a phase stepping, Fizeau type interferometer[11]. In the GII, the glass plate was placed on the metal plate with the rectangular aperture, and the inclination of the plate was adjusted until interference fringes could be seen in a monitor connected to the camera. The appropriate number and orientation of carrier fringes was then brought into the interferogram by further adjustments of the plate, and the image of this interferogram was grabbed for digital processing (Fig. 3).

As a first step in this process, the digitalized image of the interferogram was filled with zeros outside the area of the interference pattern, and subsequently "apodized", in order to obtain a smooth spectrum from it by means of a Fast Fourier Transform (FFT) algorithm (Fig. 4). The first order lobe of this spectrum was then filtered out through a window of the form

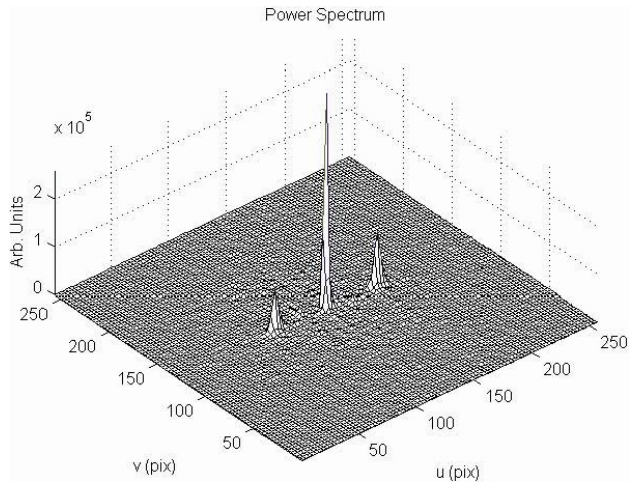


FIGURE 4. Power spectrum of the “apodized” image of the interferogram in Fig. 3.

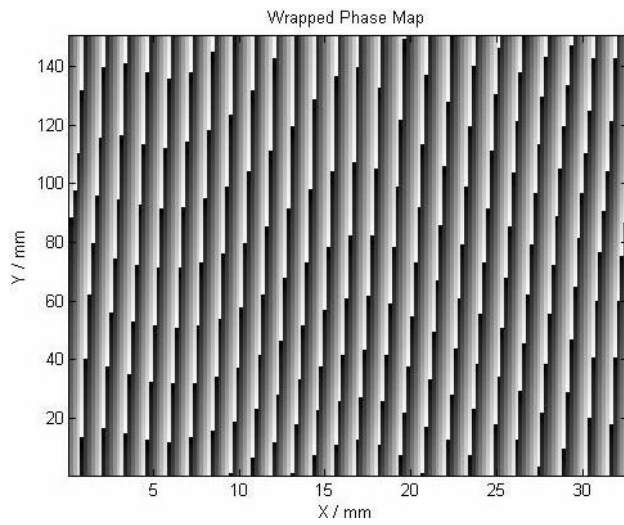


FIGURE 5. Wrapped phase map corresponding to the interferogram in Fig. 3.

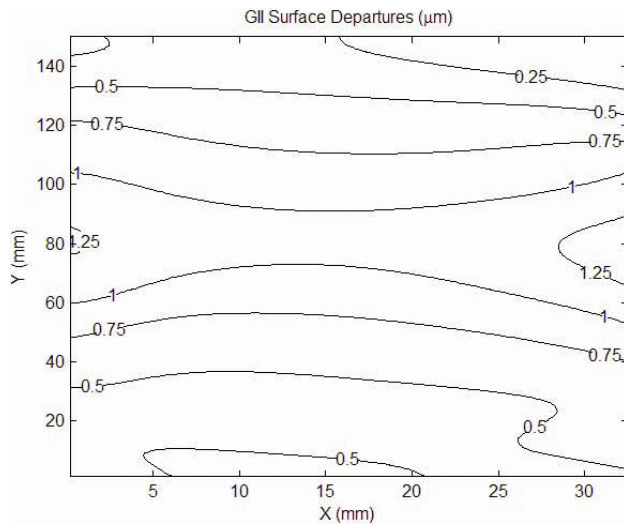


FIGURE 6. Surface topography obtained after phase-unwrapping the map in Fig. 5. The surface departures have been linked to the (X, Y) coordinates of the surface under test.

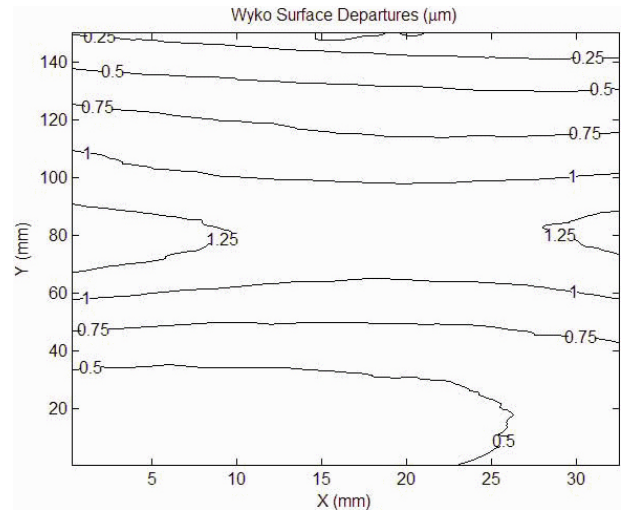


FIGURE 7. Surface topography obtained with the Wyko interferometer.

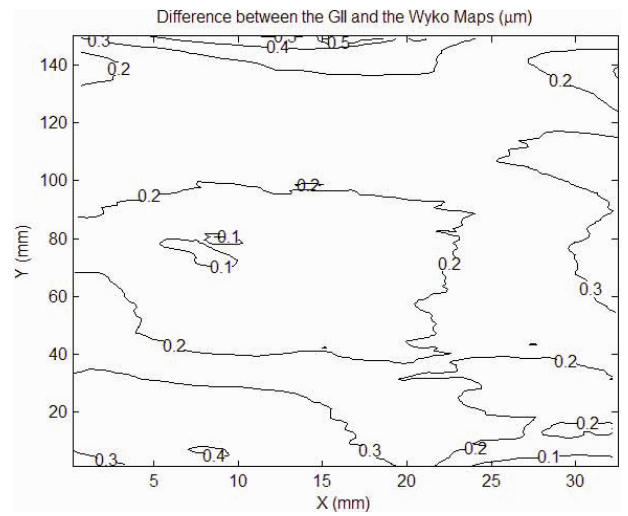


FIGURE 8. Difference between the maps in Figs. (6) and (7), after one of them was slightly rotated ($\sim 1.4^\circ$) to compensate for an inevitable error of misplacement when the surface under test was taken from the GGI to the Wyko interferometer.

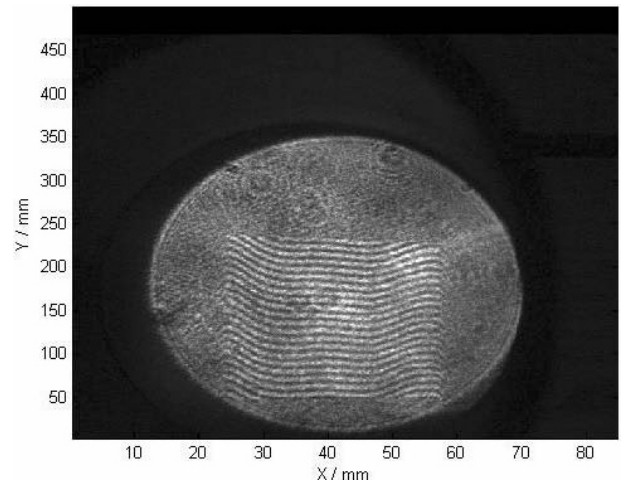


FIGURE 9. Interferogram obtained with the GII of a ground glass surface ($9 \mu\text{m}$ abrasive).

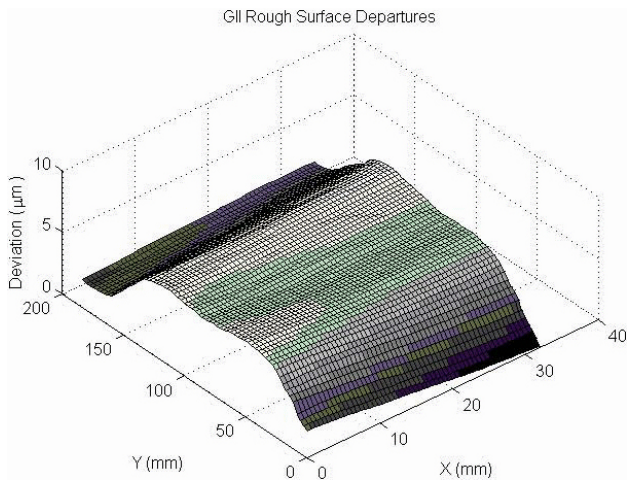


FIGURE 10. Surface topography corresponding to the interferogram in Fig. 9. The surface departures have been linked to the (X,Y) coordinates of the surface under test.

where the semi-axes a and b , which define the size of the window, are determined from inspection of the power spectrum at hand (Fig. 4). This window is, of course, a 2-dimensional version of the well known Hamming window, and was also used in the apodization process mentioned above. Now, from the filtered spectrum and Eqs. (8) and (9) we obtained the wrapped phase map associated to the interferogram (Fig. 5). The discontinuities of this map were then removed by means of a plain phase unwrapping algorithm, which consisted in adding (or subtracting) a multiple of 2π beyond a point of phase discontinuity. After this we had a continuous map of the function $\psi(x,y)$. With the values of this function and Eq. (11), we were finally able to find the map of surface departures from an ideal plane. Inevitably, a residual linear term (tilt) appears in this map, but this can easily be removed if we find the reference plane that minimizes the variance of the surface departures. To display the actual map of these, it was only necessary to transform the coordinates (x,y) of a point on the CCD to the coordinates (X,Y) of the conjugate point on the surface under test. This produced the map shown in Fig. 6.

The corresponding map obtained with the Wyko interferometer is shown in Fig. 7. The similarity between this map and the GII map is evident. The Peak-to-Valley (PV) deviation in the GGI map is $1.43 \mu\text{m}$, and the Root-Mean-Square (RMS) deviation, $0.28 \mu\text{m}$. In the Wyko map, the corre-

sponding PV and RMS deviations are $1.39 \mu\text{m}$ and $0.32 \mu\text{m}$, respectively. The difference between both maps is shown in Fig. 8. This was taken after one of the maps was slightly rotated ($\sim 1.4^\circ$), to compensate for an inevitable error of misplacement when the surface under test was taken from the GGI to the Wyko interferometer. Notice that in almost the entire inspection area the difference is lower than $0.3 \mu\text{m}$, or $\sim \lambda_{eqv}/12$.

Finally, Figs. 9 and 10 show the interferogram and the corresponding surface topography for a $185 \times 185 \text{ mm}$ ground glass surface ($9 \mu\text{m}$ abrasive). Although the precision of the map could not be independently verified with the instruments at our disposal, these figures were included in order to assure the reader that the method that we adopted to reduce the data of the GII works equally well with non-specular surfaces, in the sense that it does not require further provisions to process the data from these surfaces.

5. Conclusions

We described an interferometric method to measure surface departures from an ideal plane with a Grazing Incidence Interferometer (GII). This permits the inspection of non-specular surfaces of glass, metal and Teflon, and thus can be used to check the flatness of polishing tools. The method requires an interferogram with carrier fringes, the image of which is subsequently digitized and analyzed through Fourier and phase unwrapping techniques. The usefulness of this technique, however, is restricted to surfaces with smooth gradients; neither bumps nor holes can be measured with it. To overcome this problem, phase stepping or regularization techniques should be employed. The original design of our GII, however, prevents a simple implementation of a phase stepping mechanism. Regularization techniques were beyond the scope of this work.

Acknowledgements

The authors would like to express their gratitude to the members of the optical and the mechanical workshops at CIO, in particular to Carlos Pérez Santos, and also to Zacarías Malacara Hernández, of the Optical Engineering Group, for their assistance in various tasks that were essential for the successful completion of this work.

1. M. Gutiérrez Munguía and E. Landgrave Manjarrez, *Diseño y fabricación de un interferómetro de incidencia oblicua*, MSc Thesis, CIO (1992).
2. N. Alcalá Ochoa, G. Mendiola, E. Landgrave Manjarrez, and J.C. Sánchez Roldán, *Cuantificación de planicidad de objetos usando un interferómetro de incidencia oblicua*, Tech. Rep., CIO (2001).
3. The cemented doublets of the GII were corrected for spherical

aberration and coma for $\lambda = 0.6328 \mu\text{m}$.

4. K.H. Womack, *Opt. Eng.* **23** (1984) 391.
5. M. Takeda and K. Mutoh, *Appl. Opt.* **22** (1983) 3977.
6. N. Alcalá Ochoa, R. Rodríguez-Vera, M. Servín, and F. Mendoza Santoyo, *Opt. Commun.* **117** (1995) 213.

7. By the variance of a function $f(x, y)$ we shall mean

$$\begin{aligned} \overline{[f(x, y) - \overline{f(x, y)}]}^2 &= \overline{f(x, y)^2} - \overline{f(x, y)}^2 \\ &= \frac{1}{A} \int \int_D f(x, y)^2 dx dy - \left[\frac{1}{A} \int \int_D f(x, y) dx dy \right]^2, \end{aligned}$$

where the bar denotes average over the domain of the function $f(x, y)$, denoted here by D, and

$$A = \int \int_D dx dy$$

is the area of D. In our case, A is clearly the area under inspection.

8. K. Creath, "Temporal Phase Measurement Methods", in *Interferogram Analysis*, D.W. Robinson and G.T. Reid, Eds. (IOP Publishing, Bristol, UK, 1993) Chap. 4.

9. N. Alcalá Ochoa, J.L. Marroquín, and A. Dávila, *Opt. Commun.* **163** (1999) 15 .

10. This expression for $\psi(x, y)$ can be derived as we do in the case of interference in thin films. See, for instance, M. Born and E. Wolf, *Principles of Optics*, 6th (corrected) ed. (Pergamon, Oxford, 1984) Chap. 7, p. 286.

11. Wyko is a trademark. The Wyko interferometer is a Fizeau, phase-stepping, digital interferometer, used to test plane and spherical specular surfaces in an optical workshop.